Validation of HF radar probing of the vertical shear of surface currents by acoustic Doppler current profiler measurements

Dmitry V. Ivonin
Shirshov Institute for Oceanology, Russian Academy of Sciences, Moscow, Russia

Pierre Broche and Jean-Luc Devenon[1]
Laboratoire de Sondages Electromagnetiques de l'Environnement Terrestre, Université de Toulon et du Var, La Garde, France

Victor I. Shrira
Department of Mathematics, Keele University, Keele, UK

Received 30 June 2003; revised 22 December 2003; accepted 19 January 2004; published 1 April 2004.

[1] There exists no practical way of measuring vertical shear in the water just below the air/sea interface that contains information on air/water momentum fluxes. The paper is concerned with the validation of a recently proposed method of remote sensing of sea subsurface shear by means of a commonly used single-frequency HF radar based on the use of the second-order Bragg echo. To this end a dedicated field experiment was carried out off the French Mediterranean coast. In parallel with the HF radar probing, the independent simultaneous measurements of the subsurface shear profile were obtained by means of acoustic Doppler current profiler mounted on a floating platform, whose position was monitored by GPS. The comparison shows a fairly good agreement of the results (the discrepancy does not exceed 15%) and suggests a higher accuracy of the HF probing. *INDEX TERMS:* 4594 Oceanography: Physical: Instruments and techniques; 6959 Radio Science: Radio oceanography; 6969 Radio Science: Remote sensing; 4504 Oceanography: Physical: Air/sea interactions (0312); 4512 Oceanography: Physical: Currents; *KEYWORDS:* remote sensing and EM, currents, air/sea interactions

Citation: Ivonin, D. V., P. Broche, J.-L. Devenon, and V. I. Shrira (2004), Validation of HF radar probing of the vertical shear of surface currents by acoustic Doppler current profiler measurements, *J. Geophys. Res.*, *109*, C04003, doi:10.1029/2003JC002025.

1. Introduction

[2] The existing knowledge of fluxes at the air/water interface, which is vital for meteorology and physical oceanography, is still mostly based on indirect measuring and a mixture of modeling and guesswork. An accessible method of remote probing of vertical shear in the water just below the air/water interface which contains information on air/water momentum fluxes would be of great importance in this context. Recently, a new method of remote sensing of sea subsurface shear by means of a commonly used single-frequency HF radar based on the use of the second-order Bragg echo, has been suggested and tested experimentally [*Shrira et al.*, 2001]. The conclusion that the new method is indeed working was reached on the basis of self-consistency of the results and has not been independently verified. In the present work we address the problem of independent verification of the subsurface shear measurements obtained by the new method.

[3] The new method of probing the subsurface shear by means of HF radars is based upon an extension of the well established technique of remote sensing of surface currents employing single-frequency radars operating in high-frequency (5–30 MHz, HF) and very high frequency (50 MHz, VHF) ranges [*Barrick*, 1972; *Broche et al.*, 1987; *Paduan and Graber*, 1997]. In this range, scattering occurs in the Bragg regime; that is, the frequency spectra of radar echo reflected from the sea surface exhibit two pronounced peaks corresponding to the so-called Bragg lines (see Figure 1). The discrepancy between the observed frequency of the Bragg lines and the linear dispersion relation for resonant surface gravity waves is attributed to the Doppler shift of the frequency of surface waves due to the presence of shear current. Indeed, this shift of the surface wave frequency due to shear currents is well resolved by the radar. In the work of *Shrira et al.* [2001] the peaks both of the first and second-order Bragg backscattering were used. The following two pairs of the second-order peaks were employed: (1) the so-called "second harmonics peaks", which are mainly due to the contribution of the second harmonics of the two times longer (compared to the Bragg water wave) water waves

[1] Now at Centre d'Océanologie de Marseille, Université Mediterranée, Marseille, France.

0148-0227/04/2003JC002025$09.00

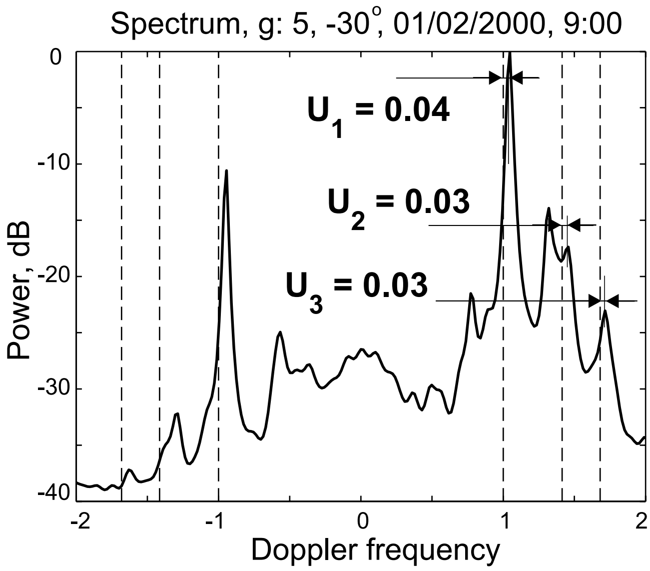

Figure 1. An example of power spectrum of 45 MHz radar sea echo averaged over NS = 48 samples recorded on 1 February 2000, 0900 UT; the frequency axis is in units of the Bragg frequency $f_B = \sqrt{2gk_0}$. The dashed vertical lines mark the unperturbed positions of (1) the first-order peaks at ± 1, (2) the harmonic peaks at $\pm\sqrt{2}$, and (3) the corner reflection peaks at $\pm 2^{3/4}$. The discrepancies between the actual and unperturbed positions of the peaks represent the magnitudes of the corresponding Doppler shifts due to the effective current U_1, U_2, and U_3 (in Bragg frequencies), respectively. See color version of this figure in the HTML.

propagating in the radar beam direction; (2) the "corner reflection peaks", which are due to a pair of oblique waves propagating at angles $\pm\pi/4$ to the radar beam and having the length equal to that of the square root of two times Bragg resonant wave.

[4] In the present work we aim at verifying the radar measurements reported by *Shrira et al.* [2001] by independent ADCP/GPS measurements carried out during the same experiment. Strictly speaking, the radar and ADCP/GPS measurements are not exactly comparable, since the times and locations of the radar and contact measurements did not always precisely coincide. However, the reasonable proximity of the observations in space and time enables us, by interpolating the results of the radar measurements, to arrive at certain conclusions both on trustworthiness of the radar results and the inherent limitations of such comparisons.

2. Theoretical Background

[5] An HF radar emits the radio wave pulses with a central wavelength λ_R. Because of the dominance of the Bragg resonance backscattering mechanism, the main peaks in the radar echo are caused by the resonant surface gravity waves of length $\lambda_R/2$ propagating to and from the radar along the radar beam with the phase velocities c_p. The main frequency of the reflected field is shifted by the frequency of the resonant surface waves $\omega = c_p k$, where $k = 2 \cdot 2\pi/\lambda_R$ is the resonant wave number. The Doppler radar measures the frequency shift $f_B = \omega/2\pi$.

[6] The dispersion relation of surface gravity waves propagating upon a horizontally uniform current with a vertical shear can be presented in the form

$$\omega = \sqrt{gk} + kU_{ef}(k)\cos\beta.$$

where ω and k are the wave angular frequency and wave number, g is the acceleration due to gravity; β is the angle between waves and the mean current; U_{ef} is the so-called effective velocity. The effective velocity, $U_{ef}(k)$, depends on the surface wave scale and in the HF radar context in most of conceivable situations is well approximated by the Stewart-Joy formula [*Stewart and Joy*, 1974]:

$$U_{ef}(k) = 2k \int_{-\infty}^{0} U(z)e^{2kz}dz. \quad (1)$$

Here $U(z)$ is the vertically sheared mean current and z is depth. So the surface waves of different scales feel the shear current differently. If we were able to measure the surface waves' frequency shift of all the lengths $U_{ef}(k)$, it would be possible to reconstruct the current profile $U(z)$.

[7] In practice, at best, there are a few values of the effective velocity $U_{ef}(k_i)$ that represent integrals of the current with different exponential weighting functions and their further interpretation must be extremely cautious without an a priori model of the profile $U(z)$ or an estimate of its vertical scale. The commonly used rule of thumb interpreting $U_{ef}(k_i)$ as the value of $U(z)$ at the depth $\lambda_i/4\pi$ is based on the result for the particular model of exponential current profile in the limit of very small shear, i.e., $U_z'/kU \ll 1$. The justification of such interpretation lies in its utmost simplicity and in the fact that it works reasonably for other monotonically decaying profiles, although under the same restricting assumption. To address the occurrence of nonmonotonic profiles we suggest to use an interpretation based upon a slightly modified rule of thumb: the effective velocity $U_{ef}(k_i)$ is interpreted as the current velocity averaged over the depth $0 \div \lambda/4\pi$. It is less sensitive to the type of profile. Thus, measuring frequency of waves of 3, 4.2, and 6 m, we will speak about current velocity averaged over depths 25, 35, and 50 cm. We emphasize that the specific values of the depths of the layers should be understood only as very rough estimates.

3. Experiment Setup

[8] To verify the radar probing of the vertical shear we obtain the effective velocity corresponding to three water wavelengths by the radar and ADCP/GPS. In the reported experiment the three effective velocities for surface waves of lengths 3, 4.2, and 6 m (see Table 1) were obtained in two independent ways: (1) by means of VHF radar; (2) by combined use of ADCP and GPS described below. We compare the results and calculate the standard deviation of the radar and ADCP/GPS discrepancy.

3.1. Radar

3.1.1. Site

[9] The field experiment was carried out by Laboratoire de Sondages Electromagnetiques de l'Environnement Ter-

Table 1. Parameters Corresponding to the Peaks

Peak	Eff. Vel.	Wave Number	Wavelength
Bragg peak	$U_1 = U_{ef}(k_1)$	$k_1 = 2\pi/\lambda_1$	$\lambda_1 = 3$ m
Second harmonic peak	$U_2 = U_{ef}(k_2)$	$k_2 = 2\pi/\lambda_2$	$\lambda_2 = 6$ m
Corner reflection peak	$U_3 = U_{ef}(k_3)$	$k_3 = 2\pi/\lambda_3$	$\lambda_3 = 4.2$ m

restre, Université de Toulon et du Var in the delta of Rhône (French Mediterranean coast) in February 2000. The site advantage is in the fact that it provides a wide range of values of vertical shear [*Broche et al.*, 1998] from very high, localized in the Rhône plume, to quite small, typical of wind induced currents, distributed in space in a constantly changing manner.

3.1.2. Technical Characteristics

[10] A VHF radar operating at 45 MHz (the EM wavelength $\lambda \simeq 6$ m and the resonant water-wave wavelength is about 3 m) was situated at a sand beach 4 km to the east of the delta (see Figure 2). The radar had 4 transmitting elements and the receiving phased array of 16 dipoles spaced by 3.33 m. The phase adjustment was made digitally at the data processing stage after the signals from each element had been separately recorded. The antenna of aperture 8λ permitted a bearing cell resolution of 6°. The directional diagrams of both the transmitting and receiving antennas were tested from a ship at the beginning of the experiment. The ship with a transmitter traversed at the distance 4 km from the radar, while the latter measured the signal. These test measurements showed that the center of the beams was recovered with an accuracy of approximately one degree, which in the context of our experiments, allows us to neglect the "antenna errors".

[11] The radar emits rectangular pulses of 4 μs or 1 μs, which corresponds to the illuminated area of 600 m or 150 m respectively. Hence the radar space resolution was 600/150 m in the along-ray and 6° in the cross-ray directions. The radar peak power is 1,6 kW enabling it to cover the range of up to 30 km under reasonably good weather and wind wave conditions. As only one radar was used, the study is confined to the radial component of the current velocity.

3.1.3. Data Processing

[12] The Welch periodogram method [*Marple*, 1987] was applied to get the power density of the sea echo. One independent sample consisted of 256 sampled points in time for 16 antennas. The Hanning window was applied to the time-frequency domain; the Chebychev window with −30 dB of sidelobe ripple was applied in the antenna angle domain. From 6 to 30 independent samples (NS) were averaged for each spectrum. It gave from 12 to 60 degrees of freedom for the spectra that resulted in a very good 95% confidence interval less than 2 dB.

3.2. ADCP/GPS Measurements

[13] The background basic water characteristics (salinity, temperature, and density) in the area of the experiment were sampled from the supporting research vessel. The vertical profile of velocity was measured from a small 1.2 m × 1.2 m × 0.2 m low-projection floating platform (see Figure 3a). It was so designed that the platform top would be at the unperturbed sea surface level or be slightly covered

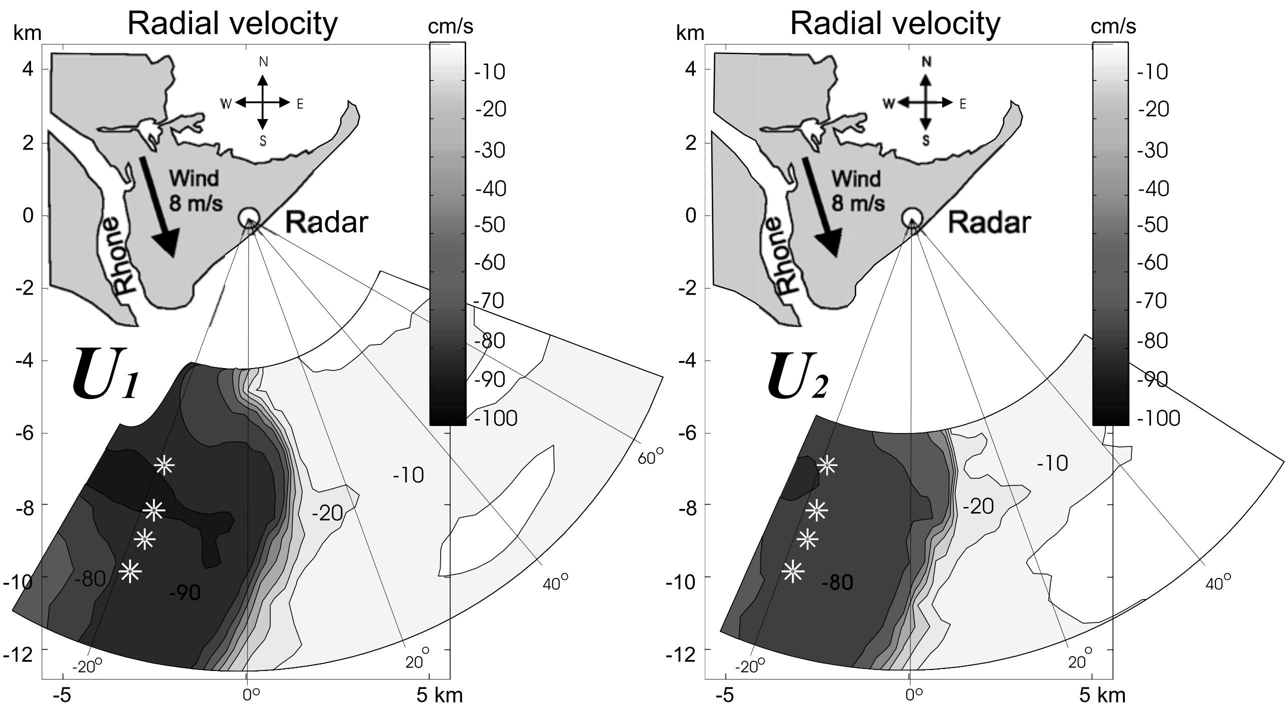

Figure 2. The radar site in the delta of Rhône (French Mediterranean coast) on 4 February 2000. The Rhône plume is seen to the southwest from the radar. The velocity fields U_1 and U_2 (radial components) were obtained from the Bragg and the second harmonics peaks, respectively. The asterisks trace the drifting platform positions from 1020 to 1115 UT (see Table 4). See color version of this figure in the HTML.

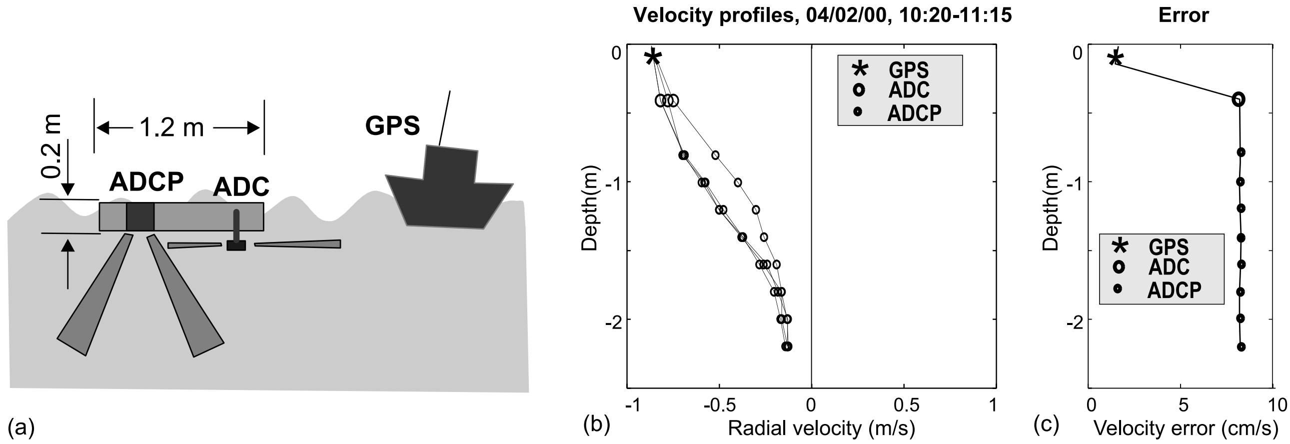

Figure 3. (a) Sketch of the ADCP/GPS measurements of vertical profile of the current velocity. The small floating platform equipped with ADC and ADCP measures relative velocity. The platform position is traced from the GPS controlled ship. (b) ADC/ADCP/GPS measurements of velocity profile $U(z)$. Four profiles from 1020 to 1115 UT (see Table 4) are shown. (c) ADC/ADCP/GPS measurement errors of velocity profile $U(z)$.

by water. Hence the windage on the platform was negligible. The floating platform was equipped with (1) an Acoustic Doppler Currentmeter (ADC) and (2) the Acoustic Doppler Current Profiler (ADCP). All the data were collected by an onboard autonomous registration system, enabling us to recover a posteriori the vertical profile of the current along the float path.

[14] The ADCP (NORTEK: frequency 3 MHz, fitted with the inside compass) measured north-south and east-west components of the horizontal velocity in the depth range 0.8 to 2.2 m with the step 0.2 m (Figure 3b). The ADC tablette (ANDERAA DCS3500: frequency 2 MHz; nominal accuracy 2 cm s^{-1}) was mounted at 20 cm depth under the platform and measured the horizontal velocity components at the depth 40 cm. Four profiles of the radial (directed from the radar) component of velocity along a platform track are shown in Figure 3b.

[15] The real accuracy of ADC/ADCP measurements from the small platform in a rough sea depends on the waveheights. To ensure a reasonably good statistics and consistency of vertical profiles, as illustrated by Figure 3b, the integration time of 10 min was chosen for the ADC/ADCP collection of each sample of vertical profile. Total error of ADC/ADCP measurements was estimated as the sum of the standard deviation of measurements during 10 min time interval and of the technical limitations of the accuracy of device (2 cm s^{-1}). It turned out that the total error increased from 2 cm s^{-1} in a calm weather to 7 cm s^{-1} for moderately rough weather with a 5–7 m s^{-1} wind. Thus the error of the ADCP measurements was estimated as 4–7 cm s^{-1}.

[16] The platform was placed in front of the Rhône mouth at 3–5 km from the radar. It was usually launched at the place where the conductivity profile showed the maximum thickness of the plume and then it drifted with the current. The ship was drifting nearby. The platform position was traced from the ship, whose position was monitored by the ship's GPS. The platform coordinates were registered each time the CTD profile was taken. The drift velocity was calculated by a regression method. If the number of points were 4 or less the linear regression was used, for more then 4 points the quadratic regression was used. The regression uncertainty of the north-south and east-west velocity components was 1–2 cm s^{-1}. It was the same for the radial velocity. The platform has the depth about 20 cm; thus its drift velocity can be estimated as that of the current at 10 cm depth. The velocities in the depth range from 40 cm to 220 cm were obtained as the vector sum of the GPS velocity and relative velocity measured by ADC/ADCP.

3.3. Errors

3.3.1. Radar Errors

[17] Here we outline the four main error factors which, in our opinion, primarily affect our estimation of the effective velocity. The radar echo results from scattering by resonant wind waves characterized by randomly distributed amplitudes and phases. In the assumption of the Gaussian-type wind wave statistics the error in the position of the peak due to this type of wave randomness is [*Barrick*, 1980]

$$\epsilon_s = (\lambda_R/4)\sqrt{\phi\, f_B/(NS \cdot T_{NS})}, \tag{2}$$

where λ_R (m) is the radar carrier wavelength, ϕ is the 3-dB width of spectral line of the normalized frequency, f_B (Hz) is the Bragg frequency, T_{NS} (s) is the observation time to integrate one independent sample and NS is the number of independent samples. The formula expresses the well known fact that the error in measuring a normally distributed random variable is inversely proportional to the square root of the number of independent samples. In our measurements the Bragg frequency f_B was 0.684 Hz, the typical value for T_{NS} was about 84 s, NS = 6 ÷ 30, the peak width ϕ was about 0.03 ÷ 0.05 (see Table 2). Hence the statistical error ϵ_s was about 0.4 ÷ 0.8 cm s^{-1}.

[18] The next possible source of error is due to the current variation. The radar spectra were obtained by 15 ÷ 40 min averaging. Moreover, sometimes, the time delay between the radar and the corresponding ADCP data collection was up to 30 min. We assume the current to be steady at the timescale of ~30 min. The investigation of the current variability

Table 2. Radar and ADCP/GPS Velocities With Errors 4 February 2000[a]

Effective Velocity	Radar, cm s^{-1}	ADCP, cm s^{-1}	ϕ, cm s^{-1}	ϵ_s, cm s^{-1}	ϵ_r, cm s^{-1}	v'_θ, cm s^{-1} grad^{-1}	ϵ_a, cm s^{-1}	ϵ_R, cm s^{-1}	ϵ_{ADCP}, cm s^{-1}	$\epsilon_t = \epsilon_R + \epsilon_{ADCP}$, cm s^{-1}
U_1	−81	−78	0.03	0.5	0.5	0.2	1.0	2.0	4.0	6.2
U_2	−70	−66	0.05	0.7	0.5	0.2	1.0	2.2	5.0	7.2
U_3	−78	−73	0.05	0.7	0.5	0.2	1.0	2.2	4.7	6.9

[a]The angle is −17, 2°, and the distance is 6.9–7.5 km.

showed that the variations do not exceed 0.5 cm s^{-1}, which we took for the upper limit

$$\epsilon_c = 0.5 \text{ cm s}^{-1}.$$

[19] The radar performs the current average over the surface patch of radial extension ~600 m. We calculate the velocities v in the nearest cells to estimate the variation of the radial current and hence the error due to it,

$$\epsilon_r = (v_{n+1} - v_{n-1})/2,$$

was usually less then 0.5 cm s^{-1}.

[20] The 16 element antenna array has the central maximum of 20° width. The half width on the level −3 dB equals $\Delta\theta$ = 5°. We estimate the error due to the limited angle resolution as

$$\epsilon_a = v'_\theta \Delta\theta.$$

The total error due to current variations over the surface patch was obtained as a mean square of the radial and angle components, $\sqrt{\epsilon_r^2 + \epsilon_a^2}$, so the total radar error was estimated as the following sum:

$$\epsilon_R = \epsilon_s + \epsilon_c + \sqrt{\epsilon_r^2 + \epsilon_a^2}. \tag{3}$$

As the experiment showed the total radar error ϵ_R was in the range 2 ÷ 3 cm s^{-1}. Characteristic values of the constituent radar errors are given in Table 2.

3.3.2. ADCP and GPS Errors

[21] On the basis of earlier measurements [*Broche et al.*, 1998] the accuracy of the ADCP velocity measurement is estimated as 7 cm s^{-1} (see Figure 3c) for wind in the range 5–7 m s^{-1} and 4 cm s^{-1} for wind in the range 2–4 m s^{-1}. The GPS velocity estimation gives the error 1–2 cm s^{-1}. As the effective velocities U_1, U_2, U_3 are obtained by integration with the corresponding weighting function of the experimental profile in accordance with equation (1) the resulting ADCP/GPS error ϵ_{ADCP} in determining the effective velocity is noticeably smaller than the ADCP error:

Peak	Wind :	2 ÷ 4 m s^{-1}	5 ÷ 7 m s^{-1}
First	$\epsilon_{ADCP}^{(1)}$:	2.5 cm s^{-1}	4.0 cm s^{-1}
Second	$\epsilon_{ADCP}^{(2)}$:	3.0 cm s^{-1}	5.0 cm s^{-1}
Third	$\epsilon_{ADCP}^{(3)}$:	2.8 cm s^{-1}	4.7 cm s^{-1},

(4)

where “1”, “2”, and “3” refer to the integration in equation (1) with wave numbers $2k_0$, k_0, and $\sqrt{2}k_0$, respectively.

4. Results

[22] The radar and ADCP measurements were compared along the floating platform track. The ADCP measurements were available from 1 to 5 February, 0900 to 1600 UT, except 3 February when the weather was stormy with a strong 15 m s^{-1} wind with gusts up to 25 m s^{-1} and the ship could not carry out measurements. The ship was available daily from 0900 to 1600 UT, which enabled us to monitor one or two platform tracks a day, each provided 4–6 samples of vertical profile.

[23] The radar measurements had the following limitations. The visibility of the secondary peaks depends strongly on the weather conditions. On 5 February there was calm weather with no wind and no waves and, no second-order peaks in the spectrum. On 2 February there was very gentle (1–2 m s^{-1}) wind and a small second-order peak (second-harmonic peak) was visible in a very narrow range of angles. The platform was launched near the edge of the plume, in the zone with very high horizontal shear of velocity, which caused a sidelobe problem, hardly resolvable for the first peaks but unresolvable for the second-order peaks. On 1 and 4 February a part of the data could not be used because of (1) the high horizontal shear causing the mentioned sidelobe problem; (2) the interference due to the peak of the dominant wind waves in the second-order radar echo, which happened to be placed too close to the second peak so that the latter could not be distinguished. An example of situation where the second harmonic peak and the peak due to the dominant wind waves are close but separated can be seen in Figure 1).

[24] The percentage of the total time of the experiment nonsuitable for the comparison and the underlying reasons are summarized in Table 3. In Table 4 we indicate the time (the day, the UT time) and coordinates (the distance from the radar and the angle, counterclockwise from the south) of ADCP profile measurements and the peak visibility for the first Bragg, the second harmonic and the corner reflection peaks. In the examples considered below we use only the samples with two or three visible peaks. Since sometimes, the time delay between the radar and the ADCP data collection was up to 30 min, we give the time of the radar and ADCP measurements separately. For the radar we also give the spatial scale over which the current was averaged. Usually, the radar in 4 μs impulse mode covered a sea patch of length 600 m but, sometimes, the echo from particular cells contained noisy signals because of landing planes, moving ships or other factors, in such circumstances the

Table 3. Percentage of Data Nonsuitable for the Comparison and the Underlying Reasons[a]

Factor Detailed	Specific Reason	Percentage
	Wind	
No wind (wind < 1 m s^{-1})	No secondary peaks	20
Stormy (wind $\geq$ 15 m s^{-1})	No ADCP measurements	20
	Limitations of Radar Signal Processing	
ADCP platform is near the edge of the plume	The problem of radar sidelobes due to the sharp horizontal gradients of velocity	10
Particular dominant frequency of wind waves ~0.2 Hz (wavelength ~40 m, wind $\geq$ 12 m s^{-1})	Interference with the second harmonic peak	20
Airplanes, ships, etc.	Noise in the VHF band	10
	Mismatch	
	Mismatch of the ADCP and radar measurements in space or time	10

[a]The specific threshold values of wind and wind waves are for the VHF radar (45 ~ MHz) only and will differ for other carrying frequencies.

statistical properties of the echo were improved by averaging the echo over two neighboring cells.

4.1. Description of the Results

[25] Below we consider an example in detail (the particular sample taken 4 February 2000, 1020 UT) and then present a summary of the results of the six comparisons we carried out. The results for 4 February 2000, 1020 UT are presented in the form of three plots in Figure 4: (1) Figure 4a shows a scaled fragment of the Doppler spectrum for the sea patch where the ADCP measurements were carried out; (2) Figure 4b presents the ADCP measurements of velocity $U(z)$; and (3) Figure 4c demonstrates the effective velocity evaluated from the ADCP measurements shown in the previous plot, and, for comparison, three points, U_1, U_2, U_3 provided by the radar.

[26] On 4 February, 1020 UT the wind was 8 m s^{-1} from the north. The Rhône plume was situated from 0° to $-50°$ and had the radial velocity about 90 cm s^{-1}. The main features of the plume can be seen in Figure 2.

[27] In the scaled fragment of the Doppler spectrum shown in Figure 4a the distance and the angle are chosen to correspond to the location of the ADCP measurements. The x axis is normalized by the frequency of the Bragg waves, f_B = 0,684 Hz. The y axis is the power density in dB. In the left upper corner of the plot specific information identifying the cell, the time and the averaging time is indicated: (1) the distance from the radar to the platform; (2) the steering angle of the radar antenna; (3) the time of radar measurements; (4) the number of averaged independent samples (NS = 30 independent samples were averaged for the spectrum in Figure 4a that resulted in the 95% confidence interval <2 dB). The peaks are marked by the solid vertical lines: the Bragg peak for λ_1 = 3 m, the second harmonic peak for λ_2 = 6 m, the corner reflection peak for λ_3 = 4.2 m. At the top of the central part of the plot three effective velocities U_1, U_2, U_3 are given in cm s^{-1}. It is easy to see that the measurements are made in the region with a strong vertical shear: the difference between the effective velocities is substantial.

[28] The ADCP/GPS measurements are given in Figure 4b. The velocity on the surface attains 90 cm s^{-1} and the shear is strong. The x axis is the radial velocity component $U(z)$. The velocity is plotted from -100 to 100 cm s^{-1}. Plus/minus indicate the velocity direction to/from the radar. The y axis is depth.

[29] The Figure 4c shows the radial component of the effective velocity $U_{ef}(k)$ as function of wave number k calculated from the ADCP measurements. We use the Stewart-Joy formula (1) and a spline interpolation for $U(z)$. The part of the profile below 2.2 m was neglected, which leads to an error for the effective velocity less than 0.1 cm s^{-1}. The radar's effective velocities are mapped for comparison: (1) $U_1 = -81$ cm s^{-1} for the Bragg wave (the value of the wave number is near 2 rad s^{-1}); (2) $U_2 = -70$ cm s^{-1} for the second harmonic (the wave number is near 1 rad m^{-1}); and (3) $U_3 = -78$ cm s^{-1} for the "corner reflection" waves (the wave numbers are near 1.4 rad m^{-1}).

[30] The available cases of the coinciding in time and space radar and ADCP/GPS observations are listed in Table 2. Their analysis is summarized below.

4.2. Comparison Between the Radar and ADCP Measurements

[31] The full comparison of all the results is presented in Figure 5. Six simultaneous radar and ADCP measurements

Table 4. Time and Coordinates for the Radar and ADCP Measurements[a]

Day	Time ADCP, UT	Distance ADCP, km	Angle deg	Time Radar, UT	Dist. radar, km	First Peak	$\sqrt{2}$ Peak	C-R Peak
1 Feb.	1019	6.38	−5.09°	1006 ÷ 1020	6.0 ÷ 6.6	+	+	+
4 Feb.	1020	7.14	−17.24°	1003 ÷ 1048	6.9 ÷ 7.5	+	+	+
4 Feb.	1045	8.45	−16.21°	1003 ÷ 1048	8.1 ÷ 8.7	+	+	−
4 Feb.	1100	9.26	−16.74°	1003 ÷ 1048	8.7 ÷ 9.3	+	+	+
4 Feb.	1115	10.21	−17.75°	1110 ÷ 1122	9.9 ÷ 10.5	+	+	+
4 Feb.	1509	3.43	−8.37°	1457 ÷ 1517	3.45 ÷ 3.75	+	+	−

[a]The peaks' existence is marked by pluses. First peak is the Bragg line; $\sqrt{2}$ peak is the second harmonic peak; and C-R peak is the corner reflection peak.

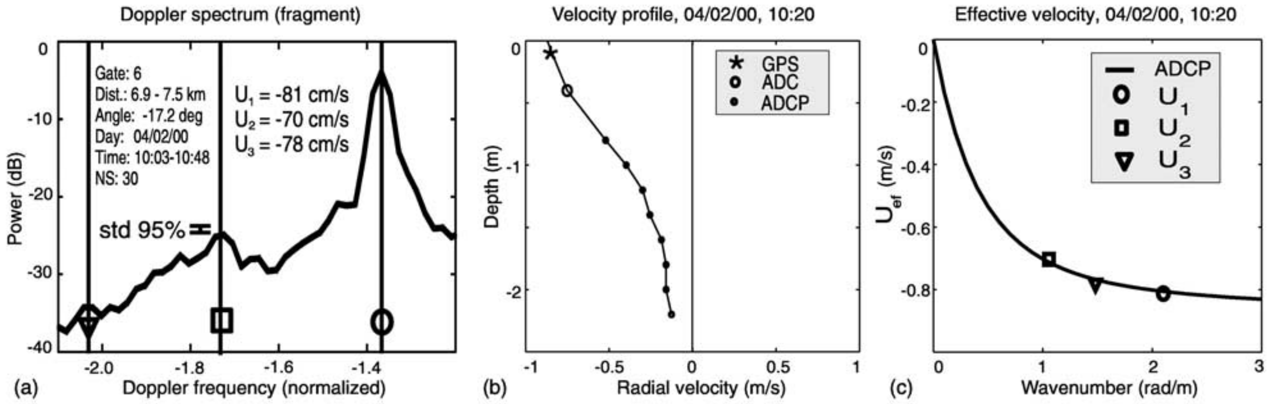

Figure 4. (a) The scaled fragment of Doppler spectrum at the bearing angle $-17, 2^0$ and distance 6.9–7.5 km on 4 February 2000. All three peaks are visible and yield $U_1 = -81$ cm s^{-1}, $U_2 = -70$ cm s^{-1}, and $U_3 = -78$ cm s^{-1}. (b) Simultaneous ADCP/GPS velocity profile measurements $U(z)$ for the same angle and distance. (c) Effective velocity, $U_{ef}(k)$, calculated from the previous plot $U(z)$. The radar's effective velocities ($U_1 = -81$ cm s^{-1}, $U_2 = -70$ cm s^{-1}, and $U_3 = -78$ cm s^{-1}) are shown for comparison.

of effective velocity are compared for each of the three effective velocities $U_1 = U_{ef}(k_1)$, U_2, U_3 discussed above. The radar measurements, U_R (y axis) are plotted versus U_{ADCP} (x axis).

[32] The results show that the mean bias is 3 cm s^{-1} from the reference line. The standard deviation with respect to the mean is 2 cm s^{-1}. The comparison of radar and ADCP results shows the discrepancy $\simeq$5 cm s^{-1}. We attribute most of the discrepancy to the ADCP error caused primarily by the floating platform agitation by surface waves.

[33] It should be noted that the two sets of measurements represent somewhat different quantities and therefore, strictly speaking, are not comparable. Given the spatial and temporal scales of the processes under consideration the ADCP/GPS data should be interpreted as instantaneous point measurements. Indeed, the characteristic integration time being $\sim$1 min implies the space integration scale $\sim$20–50 m determined by the velocity of the current. In this context the HF measurements should be viewed as time and space averaged since the characteristic time and space averaging scales of HF measurements are, as we discussed earlier, at least one order of magnitude larger. To ensure a fully justified HF radar/ADCP comparison one should use simultaneously a sufficient number of ADCP devices which would enable one to perform an ensemble averaging equivalent to the space-time averaging of the HF radars. Since this option is out of the question for obvious practical considerations, we are comparing what is possible, bearing in mind the differences in scales mentioned above. However, having said all that, fortunately, according to the commonly accepted picture of the subsurface layer variability [see, e.g., *LeBlond and Mysak*, 1978], there is a substantial slump of the variability between the scales of wind waves and swell and those of internal gravity waves, both our techniques fall into this gap. There might be a slight overlap with the high-frequency end of the internal wave spectrum but in the experiments there were no signs of internal waves. As long as there is no pronounced processes of intermediate scales (the candidates include edge waves, vorticity waves, etc.) we can expect the comparison to remain meaningful.

5. Concluding Remarks

[34] The experiment has shown a fairly good agreement between the radar and ADCP/GPS measurements of the surface vertical shear. We can conclude that the single-frequency HF radar can provide reliable estimation of two parameters of the vertical shear of the surface currents (based on measuring of the three effective velocities). Thus our main goal, the validation of the new method, has been achieved, although it would have been desirable to have a more extensive statistical base. However, the obtained data revealed that the ADCP/GPS technique is less accurate than the radar method we were validating. Both the error estimates

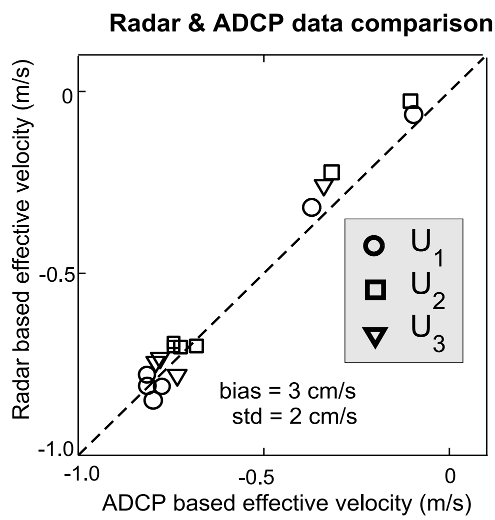

Figure 5. Comparison of ADCP and radar measurements of effective velocity. The circles are U_1; the squares are U_2; and the triangles are U_3. See color version of this figure in the HTML.

and the dispersion of the results support this conjecture. Therefore gathering a more representative statistics is likely to prove an ungratifying task. On the other hand, this suggests that at present only HF radars can measure the vertical shears in the upper meter of the sea with a good accuracy and efficiency.

[35] At its present state the technique is certainly not for operational use yet. However, we reiterate that the experiment location was chosen to test the technique for the widest range of vertical shears in the presence of the most challenging horizonal shears. The eventual aim of the proposed VHF shear probing method is in providing routine operational measurements of relatively weak vertical shears typical of the wind-driven currents and, on their basis, monitoring the air/sea momentum exchange. From this perspective, we conclude, that we have got encouraging preliminary results, and the task of further perfecting the VHF shear probing looks feasible.

[36] **Acknowledgments.** The work was supported by INTAS Fellowship YSF01/1-181, INTAS 01-234, Russian Science Support Foundation, and Russian Foundation for Basic Research N01-05-64603, N02-05-65140, and N03-05-06162.

References

Barrick, D. (1972), Remote sensing of sea state by radar, in *Remote Sensing of the Troposphere*, edited by V. Derr, chap. 12, pp. 1–46, U.S. Govt. Print. Off., Washington, D. C.

Barrick, D. E. (1980), Accuracy of parameter extraction from sample-averaged sea-echo Doppler spectra, *IEEE Trans. Antennas Propagt.*, *28*, 1–10.

Broche, P., P. Forget, J. C. de Maistre, J. L. Devenon, and M. Crochet (1987), VHF radar for ocean surface current and sea state remote sensing, *Radio Science*, *22*, 69–75.

Broche, P., J. L. Devenon, P. Forget, J. C. de Maistre, J. J. Naudin, and G. Cauwet (1998), Experimental study of the Rhone plume. part I: Physics and dynamics, *Oceanol. Acta*, *21*, 725–738.

LeBlond, P. H., and L. A. Mysak (1978), *Waves in the Ocean*, Elsevier Sci., New York.

Marple, L. S. (1987), *Digital Spectral Analysis: With Applications*, Prentice Hall, Englewood Cliffs, N. J.

Paduan, J. D., and H. C. Graber (1997), Introduction to high-frequency radar: Reality and myth, *Oceanography*, *10*, 36–39.

Shrira, V. I., D. V. Ivonin, P. Broche, and J. C. de Maistre (2001), On remote sensing of vertical shear of ocean surface currents by means of a single-frequency VHF radar, *Geophys. Res. Lett.*, *28*, 3955–3958.

Stewart, R. H., and J. W. Joy (1974), HF radio measurements of surface currents, *Deep Sea Res.*, *21*, 1039–1049.

J.-L. Devenon, COM, Université Mediterranée, rue de la Batterie des Lions, 13007 Marseille, France. (devenon@com.univ-mrs.fr)

P. Broche, LSEET, Université de Toulon et du Var, 83957 La Garde, France. (broche@lseet.univ-tln.fr)

D. V. Ivonin, Shirshov Institute for Oceanology, Russian Academy of Sciences, 36 Nakhimovsky av., Moscow 117851, Russia. (dima@wave.sio.rssi.ru)

V. I. Shrira, Department of Mathematics, Keele University, Keele ST5 5BG, UK. (v.i.shrira@keele.ac.uk)